Electronic Supplementary Material (ESI) for ChemComm.

High-temperature Electron Transfer Coupled Spin Transition (ETCST) with Hysteresis in a Discrete [Fe_2Co_2] Prussian Blue Analogue

Jyoti Yadav, Dibya Jyoti Mondal, Sanjit Konar*

Department of Chemistry, Indian Institute of Science Education and Research Bhopal
Madhya Pradesh, India 462066
E-mail: skonar@iiserb.ac.in

Table of Contents

Experimental Procedures:

1. Materials:

In metal salts, Cobalt (II) perchlorate hexahydrate and Ferric chloride were purchased from Alfa-Aesar and Merck respectively and used as received. All other chemicals Potassium tris(1-Pyrazolyl) borohydride, Benzyl Bromide, Ethylenediamine, 2-Pyridinecarboxaldehyde were persuaded from Sigma- Aldrich. Sodium Cyanide is from Loba Chemie. All solvents used were at least reagent grade. All the reactions were performed in atmospheric air.

Caution! Cyanides are very much toxic, therefore, it should be handled with great care and precautions. The unreacted cyanides and the glassware's used for the cyanide reaction was quenched by aqueous solution of KMnO4. Since perchlorates are highly explosive in nature, heating was done carefully, if required.

2. Synthetic procedures:

2.1. Synthesis of $Na[Fe(Tp)(CN)_3]$:

The Fe-CN complex was prepared according to earlier procedure reported.[1] Instead of KCN, NaCN was used. IR: ν_{CN} = 2126 cm^{-1}

2.2. Synthesis of {en(Bn)py}]:

The tetradentate N-donor ligand was prepared using previously reported method.[2] IR (cm^{-1}): ν_{CH} = 2812(as), 2796(s); $\nu_{C=N}$ = 2355(w); $\nu_{C=C}$ = 1590(m); ν_{C-N} = 1239(m).

2.3. Synthesis of $[Fe(Tp)(CN)_3]_2[Co\{en(Bn)py\}]_2(ClO_4)_2 \bullet 4MeOH \bullet 4H_2O$ (1•4MeOH•4H_2O):

1•4MeOH•4H_2O was prepared by dropwise addition of methanolic solution of in-situ prepared $[Co\{en(Bn)py\}Sol_2](ClO_4)_2$ complex to aqueous solution of $Na[Fe(Tp)(CN)_3]$ in 1:1 stoichiometric ratio. Dark green crystals suitable for X-ray diffraction were obtained upon slow evaporation of the filtrate at room temperature.
IR (cm^{-1}): ν_{CN}(bridged) = 2087, 2059 and 2116 cm^{-1}
Elemental Analysis: (Experimental) N = 18.78%, C = 48.75% and H = 4.92%; Calculated: C = 49.07%, H = 5.10% and N = 18.71%.

2.4 Solvent exchange procedure:

The process of solvent exchange was done by redissolving complex-**1** in different solvents and further characterized by elemental analysis, Infrared spectroscopy and thermogravimetric analysis.

a) 1•4H_2O: (experimental) N = 19.64%, C = 51.80%, H = 4.36%; Calculated: C = 51.78%, H = 4.35%, N = 19.62%.
b) 1•2MeCN : (experimental) N= 20.22%, C = 52.15%, H = 4.50%; Calculated: C = 52.06%, H = 4.47%, N = 20.24%.

c) 1•3EtOH : (experimental) N = 18.33%, C = 51.88%, H = 5.04%; Calculated: C = 51.80%, H = 4.95%, N = 18.24%.
b) 1•Acetone : (experimental) N = 19.18%, C = 52.06%, H = 5.62%; Calculated: C = 52.09%, H = 4.53%, N = 19.03%.
b) 1•3DCM : (experimental) N = 17.32%, C = 47.25%, H = 4.1775%; Calculated: C = 47.23%, H = 4.11%, N = 17.26%.

2.5. Desolvated Complexes:

The desolvation process was done by keeping freshly prepared samples at 60°C under high vacuum for about 24 hours. Complete loss of solvents was characterised by elemental analysis and infrared spectroscopy.
a) 1 : Experimental: C = 51.79%, H = 4.36%, N = 19.63%; Calculated: C = 51.78%, H = 4.35%, N = 19.62%.
b) 1': Experimental: C = 50.86%, H = 4.06%, N = 19.55%; Calculated: C = 51.78%, H = 4.35%, N = 19.62%.
c) 1'': Experimental: C = 50.51%, H = 4.27%, N = 19.25%; Calculated: C = 51.78%, H = 4.35%, N = 19.62%.
d) $1^{3'}$: Experimental: C = 50.90%, H = 4.27%, N = 19.84%; Calculated: C = 51.78%, H = 4.35%, N = 19.62%.
e) $1^{4'}$: Experimental: C = 51.09%, H = 4.26%, N = 19.55%; Calculated: C = 51.78%, H = 4.35%, N = 19.62%.
f) $1^{5'}$: Experimental: C = 50.99%, H = 4.26%, N = 19.63%; Calculated: C = 51.78%, H = 4.35%, N = 19.62%.

3. Physical measurements:

3.1. Crystal Data Collection and Structure Determination:
Intensity data were collected on a 'Bruker D8-Venture' diffractometer using a graphite monochromated MoKα radiation (λ = 0.71073) at 140 K. Data collections were performed using ϕ and ω scan. Olex2 was used as the graphical interface and the structures were solved with olex2.solve structure solution program using Charge Flipping and refined with the ShelXL refinement package using Least-Squares minimisation. All non- hydrogen atoms were refined anisotropically.

3.2. Powder X-ray Diffraction study:
Powder X-ray diffractometer was carried for the homogenously crushed crystals of the samples in an AntonPaar in Argon gas flow fitted in a PANalytical X'Pert Pro diffractometer at room temperature with 2θ ranging from 5 to 50.

3.3. Squid Magnetometry Study:
The magnetic study has been performed using SQUID-VSM magnetometer. All samples were grinded properly before measuring magnetic moment vs. temperature data, to minimize the reorientation of the crystalline particles under applied DC field. All the measurement has been performed with an applied DC field of 1000 Oe from 200-390 K temperature range. The measured values were corrected for the experimentally measured contribution of the sample holder and the derived susceptibilities were corrected for the diamagnetism of the samples, estimated from Pascal's tables.

3.4. Magnetic data fitting:

The magnetic data in all cases were fitted by using Slichter-Drickamer mean-field model by using equation:[3a]

$$\ln\left[\frac{1-\gamma_{HS}}{\gamma_{HS}-f_{HS}}\right] = \frac{\Delta H + \Gamma(1+f_{HS}-2\gamma_{HS})}{RT} - \frac{\Delta S}{R} \ldots\ldots\ldots\ldots (1)$$

Where, γ_{HS} represents the mole fraction of molecules in high spin state; f_{HS} is residual mole fraction of high spin species which do not show spin transition even at low temperature; ΔH and ΔS are variation in enthalpy and entropy during spin transition; Γ represents the interaction energy between the molecules (cooperativity); R is the Universal Gas constant and T is the temperature. The quantities γ_{HS} and f_{HS} can be expressed as a function of $\chi_M T$ product which are as follows:

$$\gamma_{HS} = \frac{(\chi_M T)_m - (\chi_M T)_{LS}}{(\chi_M T)_{HS} - (\chi_M T)_{LS}} \ldots\ldots\ldots\ldots (2)$$

$$f_{HS} = \frac{(\chi_M T)_R - (\chi_M T)_{LS}}{(\chi_M T)_{HS} - (\chi_M T)_{LS}} \ldots\ldots\ldots\ldots (3)$$

Here, $(\chi_M T)$m corresponds $\chi_M T$ value at any certain temperature; $(\chi_M T)_R$ is the residual fraction of Fe(III) low spin and Co(II) high spin present at low temperature; and $(\chi_M T)_{HS}$ and

$(\chi_M T)_{LS}$ represents the $\chi_M T$ value at absolutely populated high spin and low spin species of the molecule respectively.

3.5. Differential Scanning Calorimetric Study:

The Differential Scanning Calorimetric study was performed on PerkinElmer, Pyris 6 type DSC 6000 instrument. Data collected and baseline correction was done using software version 11.0.0.0449. The data measurement was taken from 250 K to 413 K at a scan rate of 6 K/min.

3.6. LIESST measurement:

The LIESST measurement was done by tape-method. The sample (~22.5 mg.) was firstly spread on a [2 cm × 2 cm] tape & placed inside a plastic tube, followed by the green light (532nm.) irradiation for 6 hours at 5 K temp. Under 0.5 T magnetic field until the magnetic moment signal of the sample got Saturated. Afterwards, the sample was scanned from 5K to 400K with the scan rate of 3 K/min (heating mode) & then 400K to 5K with similar scan rate (cooling mode).

3.7. Thermogravimetric Analysis:

The Thermogravimetric Analysis was performed on PerkinElmer instrument at a scan rate of 5 K/min.

3.8. FT-Infrared Spectroscopy study:

FT-IR spectra were recorded by using a Perkin-Elmer Spectrum BX Spectrometer on KBr pellets with wavenumber ranging between 4000 cm^{-1} - 400 cm^{-1}.

3.9. Variable Temperature Infrared Spectroscopy:

Variable Temperature FT-IR was recorded with same spectrometer by providing external heat from hot air gun on the KBr pellet of the sample.

3.10. Cyclic Voltammetry Study:

The electrochemical study of the sample was measured by using VersaSTAT-3 instrument using software VersaStudio. The study was done by using three-electrode system consisting of glassy carbon as working electrode, Pt wire as a counter electrode and Ag/AgCl electrode as a reference electrode. 1 × 10^{-4} M concentration of **1**•4MeOH•$4H_2O$ and 2 × 10^{-4} M concentration of its constituent metal complexes ($Na[Fe(Tp)(CN)_3]$ and $[Co(L)(Sol)_2]$ were used for the data collection and 0.1 M of $[N(Bu)_4]BF_4$ was used as supporting electrolyte in Methanol. The scan range for the sample solutions were from -0.70 to +1.3 V. The scanning cycle was performed by initiating with reduction followed by oxidation. The measurement was performed at a scan rate of 0.05 V/s at room temperature. For **1**•4MeOH•$4H_2O$, measurement was performed at different scan rates (Figure S14b) keeping same concentration of 1 × 10^{-4} M. All the potentials were measured with respect to Ferrocene/Ferrocenium redox couple.

3.11. UV-Visible Spectroscopy:

The solid as well as solution phase UV-Visible spectroscopic data was collected using Cary 100 instrument using Scan Software Version 4.20(468) scanning between wavelength 300 nm to 1200 nm.

Results and Discussion:

1. Crystal Structure Determination:

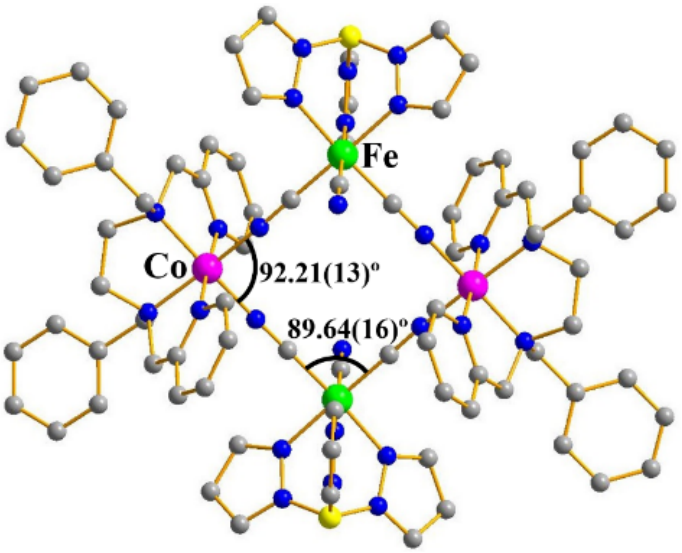

Figure S1. Crystal Structure of **1**•4MeOH•4H_2O. Colour Code: Green: Fe; Pink: Co; Blue: N; Grey: C; Yellow: B. Solvent and anions are omitted for clarity. (CCDC 1983861)

Table S1. Crystallographic data:

Identification code	**1**
Empirical formula	$C_{42}H_{48.97}BClCoFeN_{13}O_8$
Formula weight	1024.94
Temperature/K	140.0
Crystal system	monoclinic
Space group	P21/c
a/Å	13.6224(9)
b/Å	16.1549(10)
c/Å	22.4930(16)
α/°	90
β/°	105.752(3)
γ/°	90
Volume/$Å^3$	4764.1(6)
Z	4
Dx,g cm^{-3}	1.429
R_1[a]	0.0546
wR_2[a]	0.0993

[a] $I \geq 2\sigma(I)$: $R_1 = \Sigma||F_o| - |Fc||/\Sigma|F_o|$, $wR_2 = \{\Sigma[w(Fo_2 - Fc^2)^2]/\Sigma[w(Fo^2)^2]\}^{1/2}$.

Table S2. Selected bond lengths at 140 K:

Atom	Atom	Length/Å
Co1	N12	2.002(3)
Co1	N13	1.944(3)
Co1	N10	1.941(3)
Co1	N11	2.000(3)
Co1	N8	1.886(4)
Co1	N7	1.884(3)
Fe1	N1	2.001(3)
Fe1	N5	2.013(3)
Fe1	N3	2.007(3)
Fe1	C11	1.858(4)
Fe1	C10	1.866(5)
Fe1	C12	1.901(5)

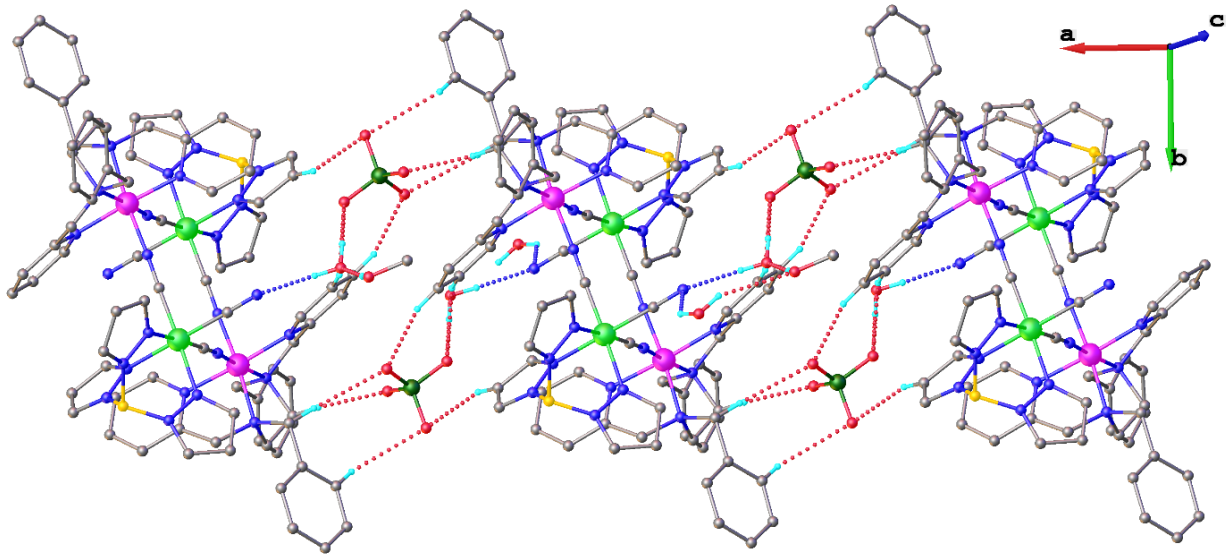

Figure S2. Hydrogen bonding interactions between solvent molecules, perchlorate anions and the [Fe_2(μ-CN)Co_2] square grids. The Hydrogen atoms not involved in Hydrogen bonding and the minor disordered components of the solvent molecules have been omitted for clarity.

2. Powder X-ray Diffraction measurement:

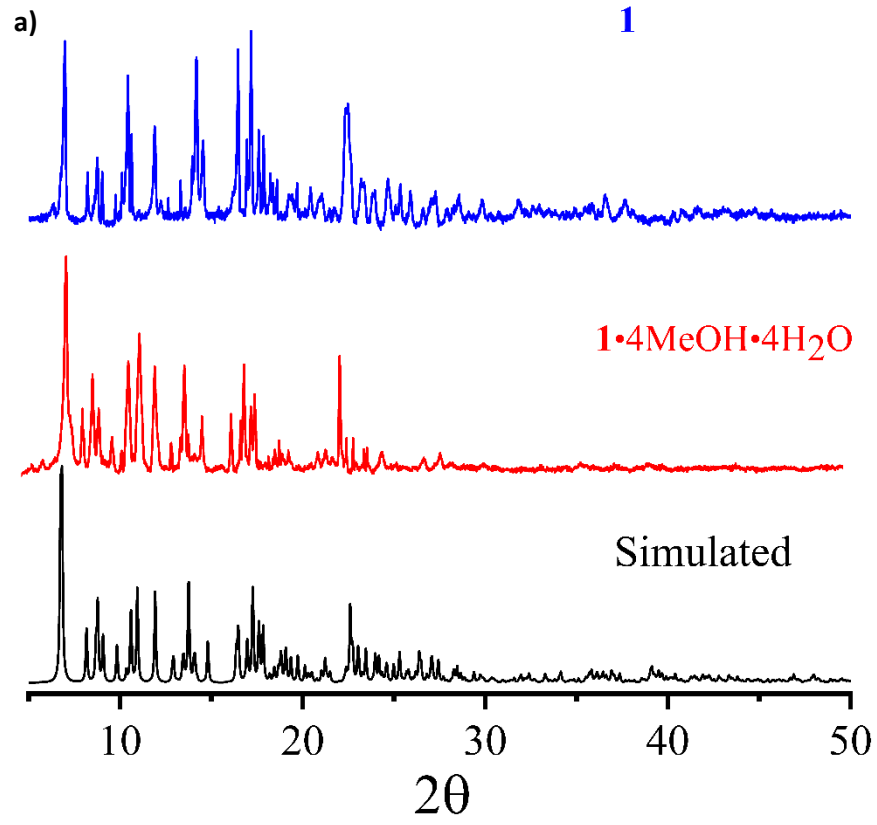

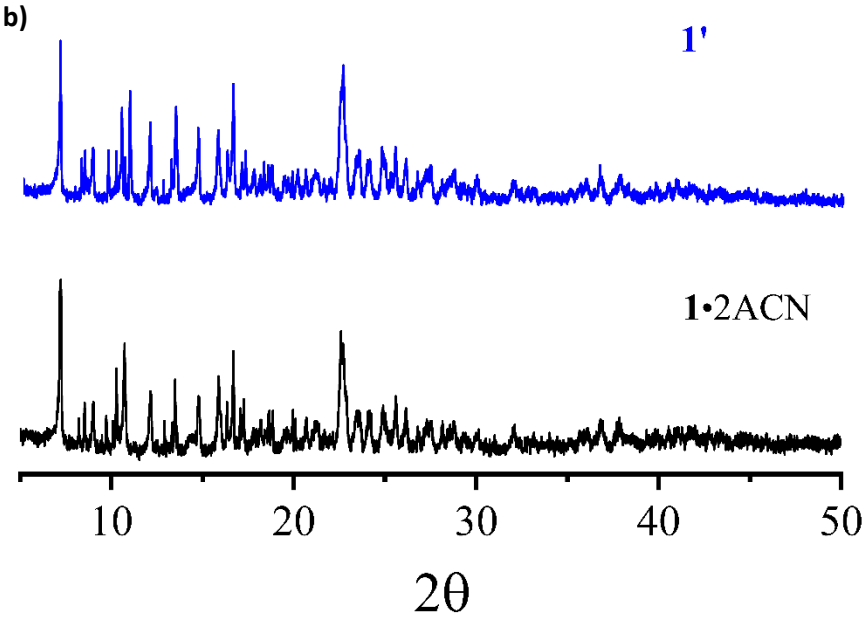

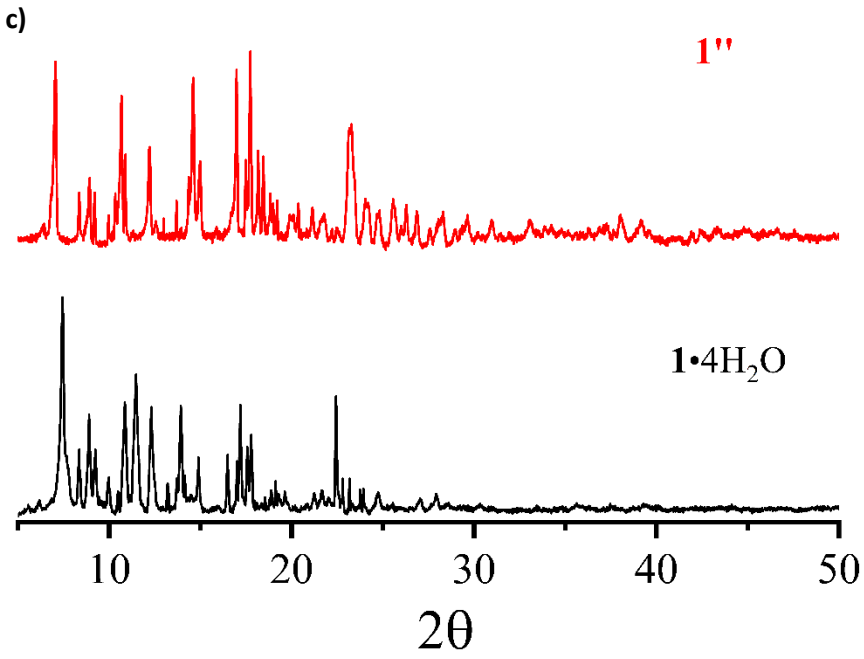

Figure S3. P-XRD data for a) **1**•4MeOH•4H_2O & **1**, b) **1**•2MeCN & **1'** and c) **1**•4H_2O & **1"** between 2θ ranging from 5 to 50 at room temperature (298 K).

P-XRD patterns for the as synthesized sample, the solvatomorphs and their respective desolvated forms at lower 2θ range shows similar trend as of the SC-XRD simulated powder data of **1**•4MeOH•4H_2O. Thus, it is supposed that the structural integrity as well as phase purity of the samples are retained all through the various characterizations and measurements.

3. Magnetic Measurements:

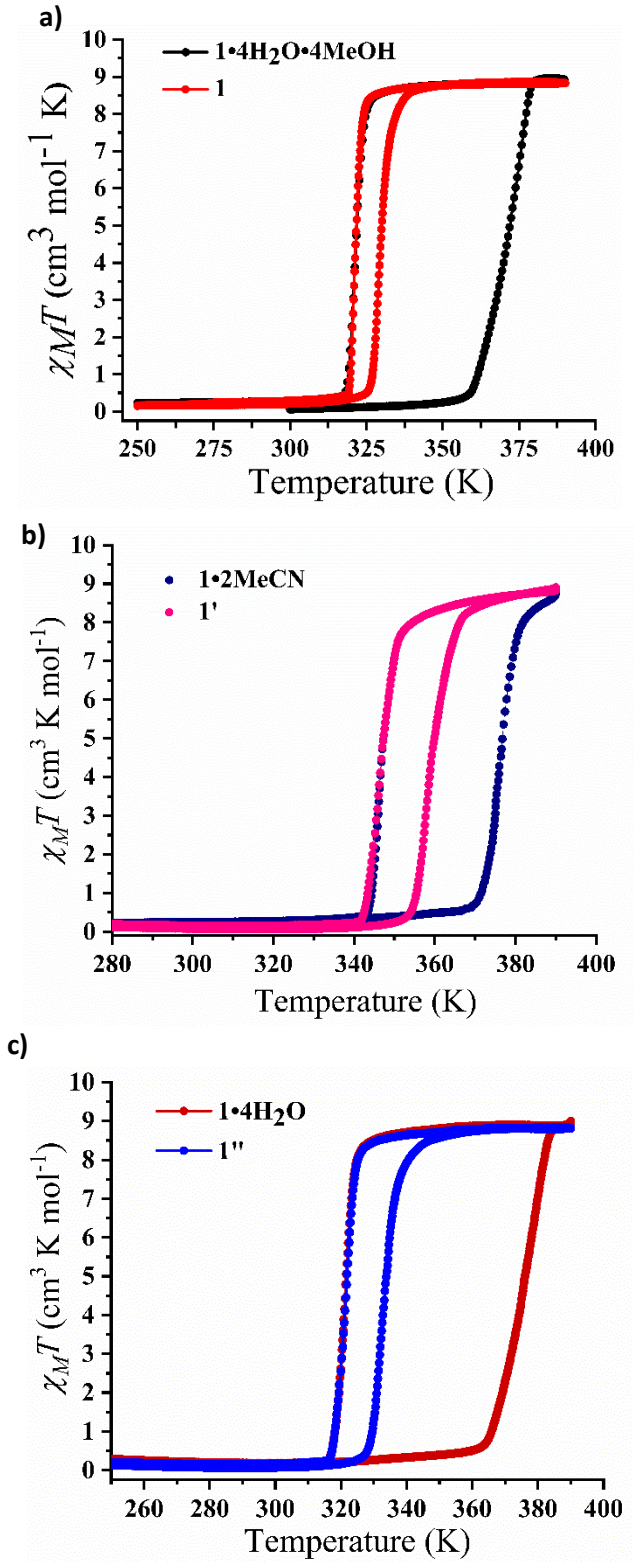

Figure S4. $\chi_M T$ *vs* T plot for a) **1**•4MeOH•4H_2O & **1**, b) **1**•2MeCN & **1'** and c) **1**•4H_2O & **1"** between 2 K to 390 K at a scan rate of 6 K/min.

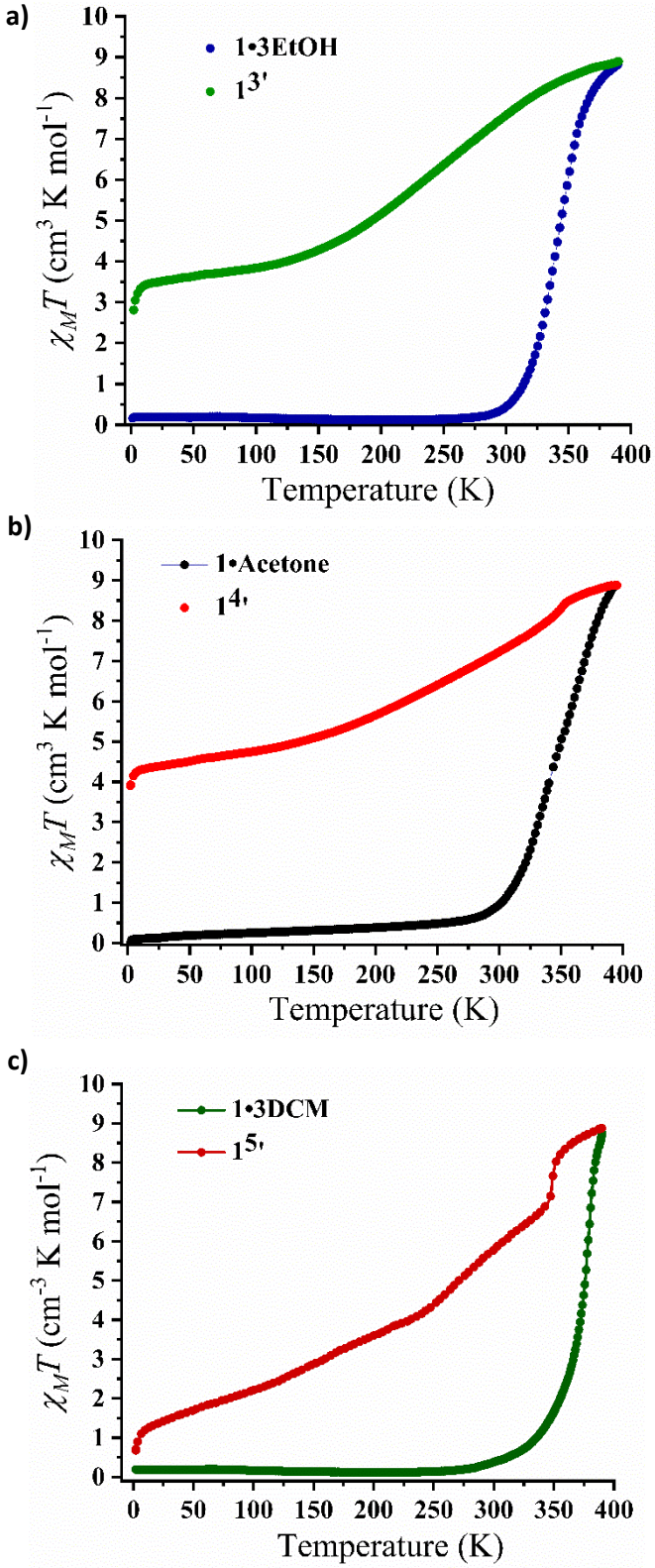

Figure S5. $\chi_M T$ *vs* T plot for a) **1**•3EtOH & **1$^{3\prime}$**, b) **1**•Acetone & **1$^{4\prime}$** and c) **1**•3DCM & **1$^{5\prime}$** between 2 K to 390 K at a scan rate of 6 K/min.

4. Magnetic data fitting:

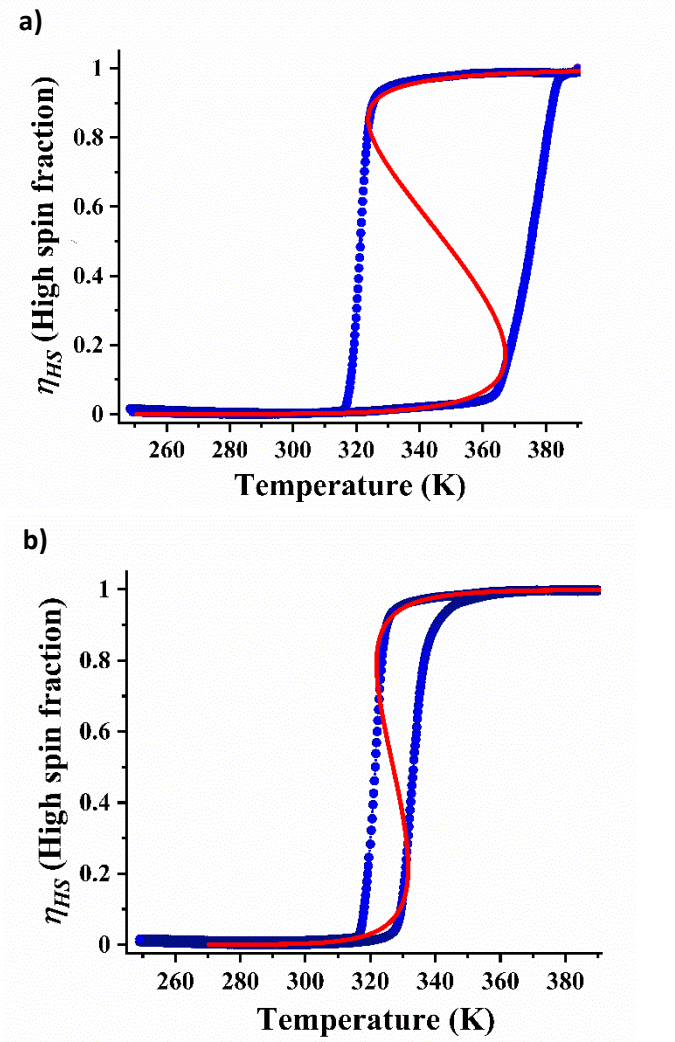

Figure S6. η_{HS} *vs* T fitting data for a) **1**•4H_2O and b) **1''**.

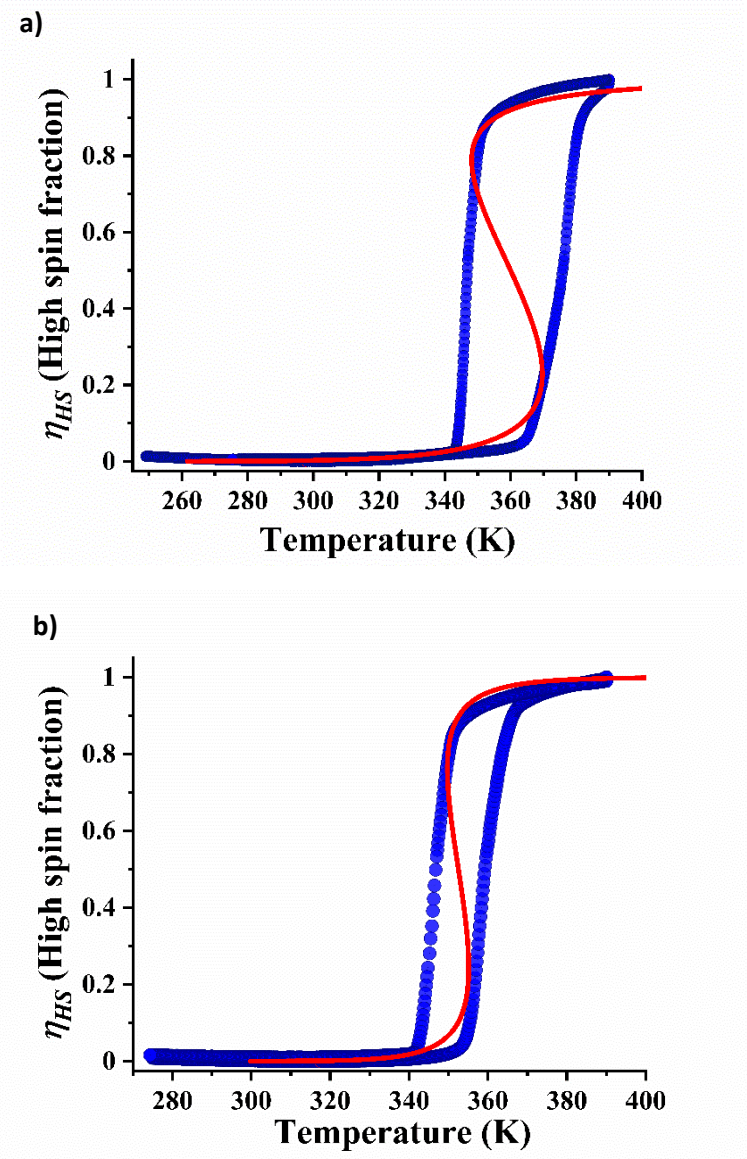

Figure S7. η_{HS} *vs* T fitting data for a) **1**•2MeCN and b) **1'**.

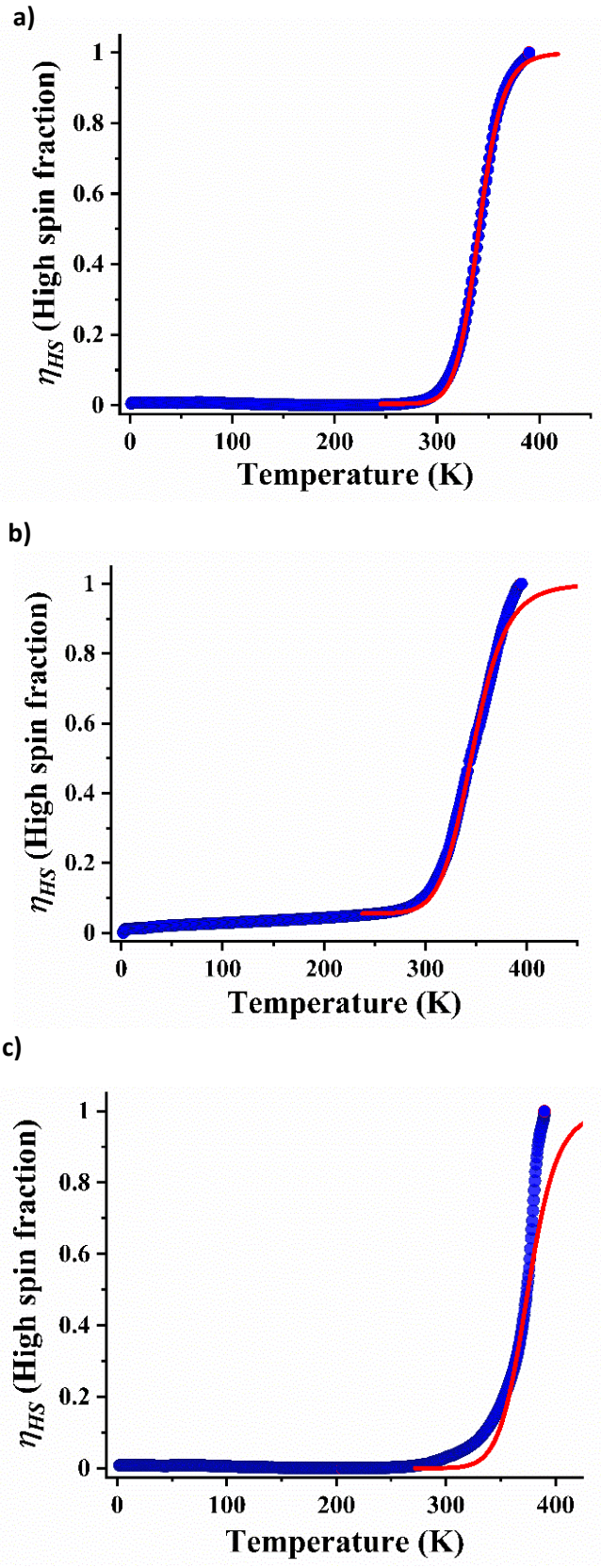

Figure S8. η_{HS} *vs* T plot for a) **1**•3EtOH, b) **1**•Acetone and c) **1**•3DCM.

Table S3. Thermodynamical parameters obtained from the simulation of the experimental $\chi_M T$ *vs* T curve.

Complex	ΔS_{avg} (J/K mol)	ΔH_{avg} (kJ/mol)	$T_{1/2avg}$ (K)	Γ (kJ/mol)	γ^R_{HS}
1•2MeCN	102.21	36.795	360	8.7	0
1′	389.26	13.702	352	8	0
1•4H_2O	119.28	41.509	348	10.8	0
1″	226.84	74.177	327	8.1	0
1•3EtOH	244.09	83.235	341	0	0.004
1•Acetone	176.74	61.329	347	0	0.05
1•3DCM	233.21	87.454	375	0	0

The thermodynamic parameters ΔS and ΔH calculated from the magnetic data fitting and that from the DSC are in good agreement with the transition temperatures obtained in all the samples (Figure S9, page no. 17-19). For the molecules exhibiting spin transition between HS and LS states, a local strain gets created due to expansion or contraction of the molecular volume. This leads to change in degree of cooperativity between the molecules via intermolecular interactions. Thus, the interaction parameter (Γ) values gives the explanation of the presence of hysteresis in the complexes where Γ > 0.

5. **Differential Scanning Calorimetric Study:**

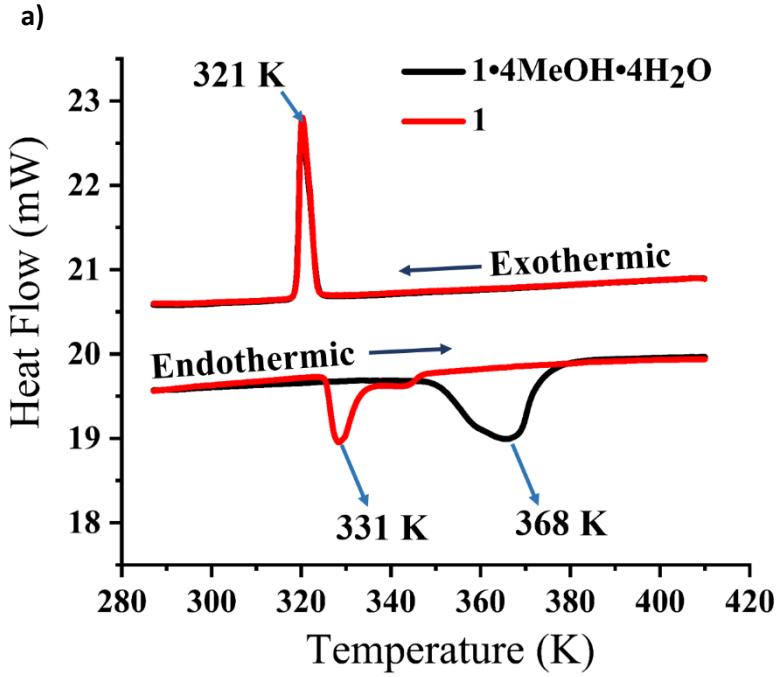

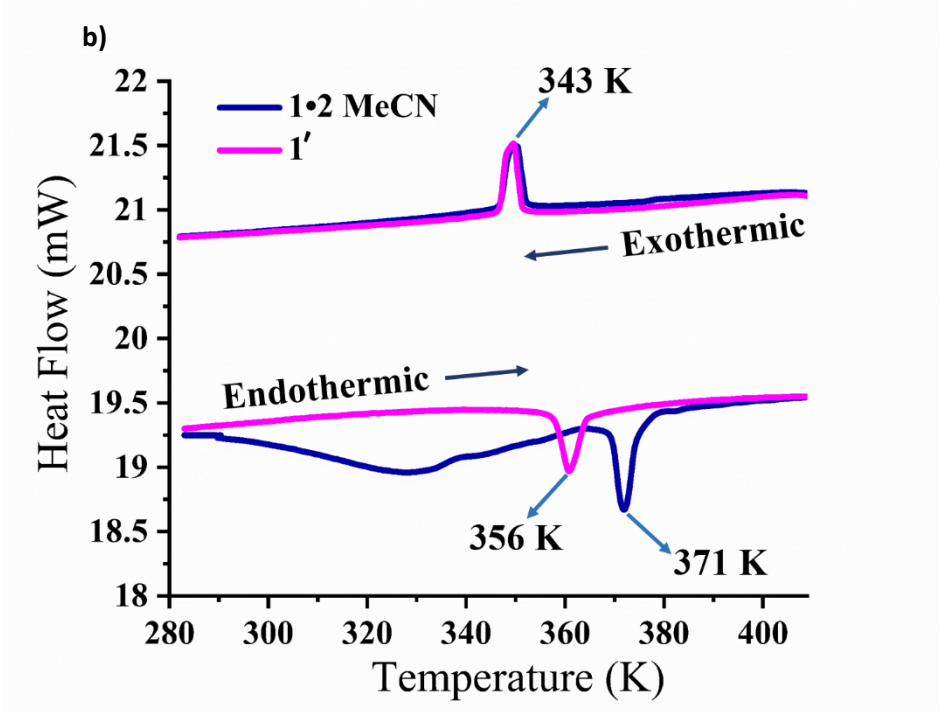

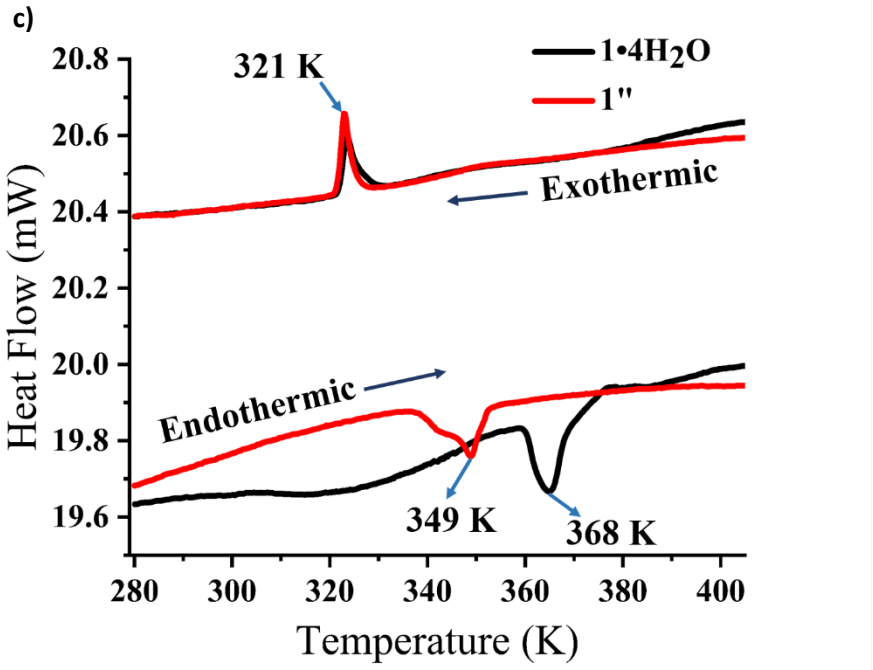
c)
321 K
1•4H2O
1''
Exothermic
Endothermic
349 K
368 K
Heat Flow (mW)
Temperature (K)

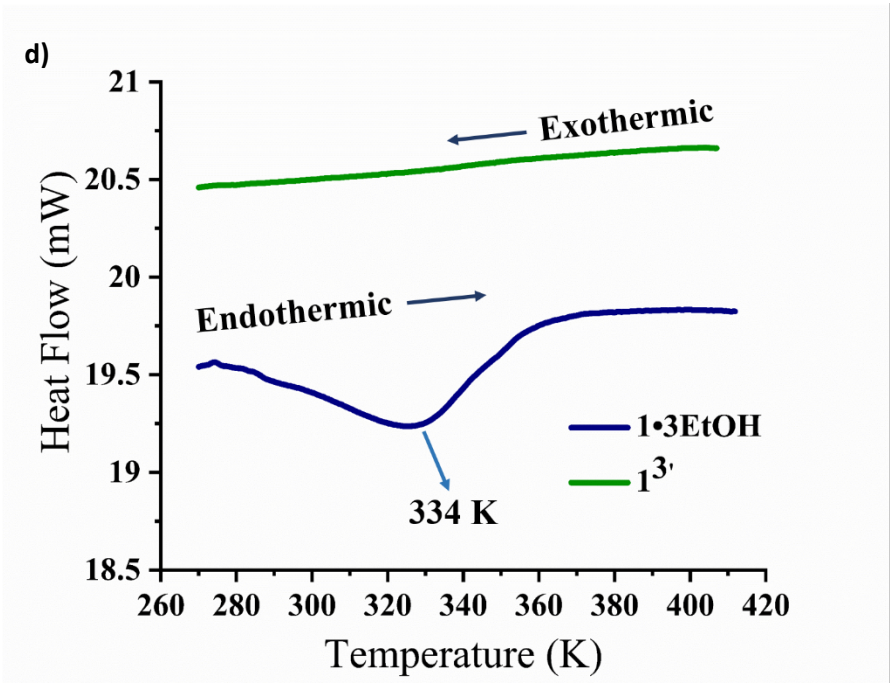
d)
Exothermic
Endothermic
1•3EtOH
1^3'
334 K
Heat Flow (mW)
Temperature (K)

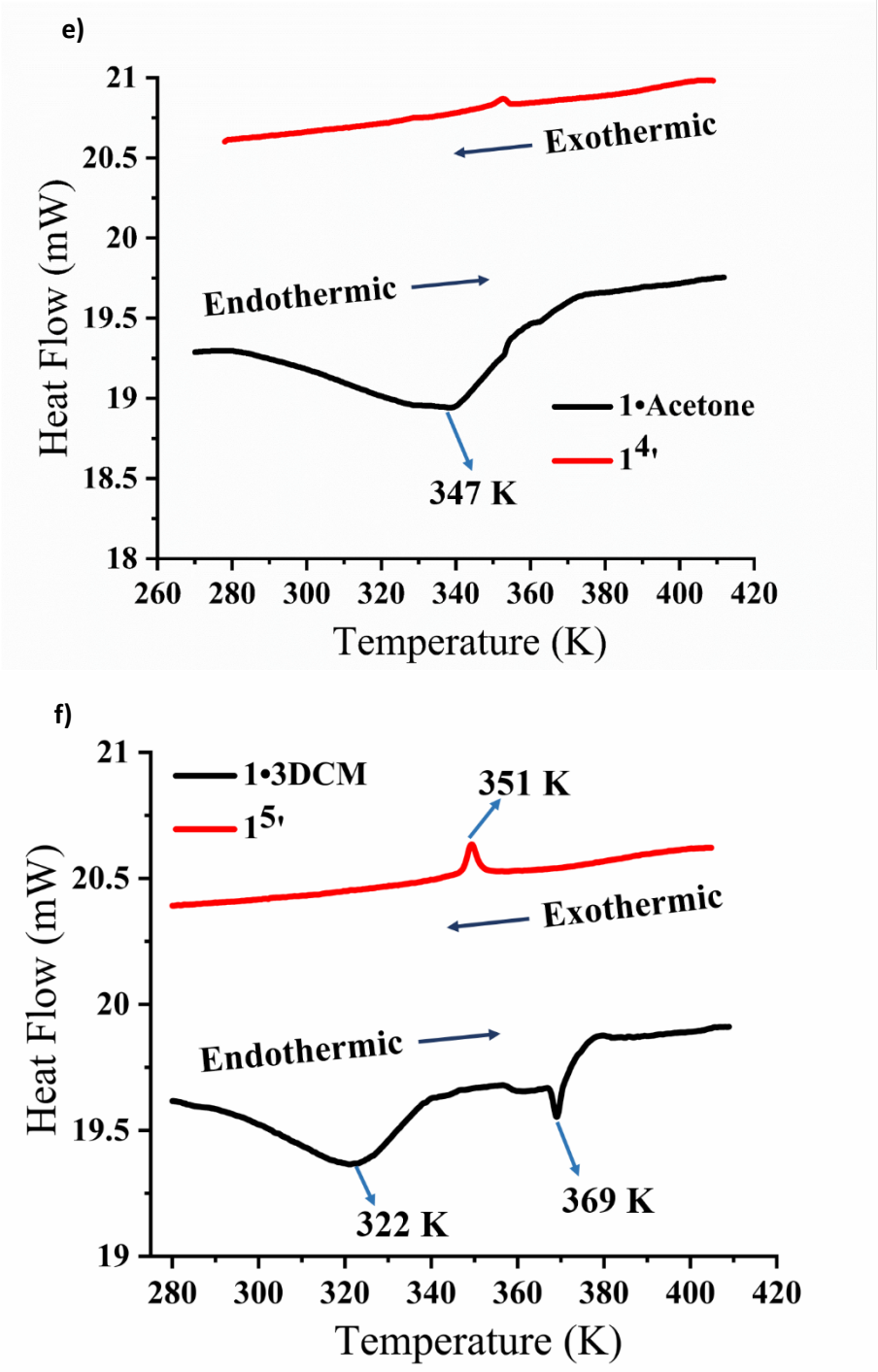

Figure S9. DSC data plot for a) **1**•4MeOH•4H_2O and **1** b) **1**•2MeCN and **1'**, c) **1**•4H_2O and **1"**, b) **1**•3EtOH, c) **1**•Acetone and d) **1**•3DCM complexes.

6. Light Induced Excited Spin State Trapping (LIESST) measurement:

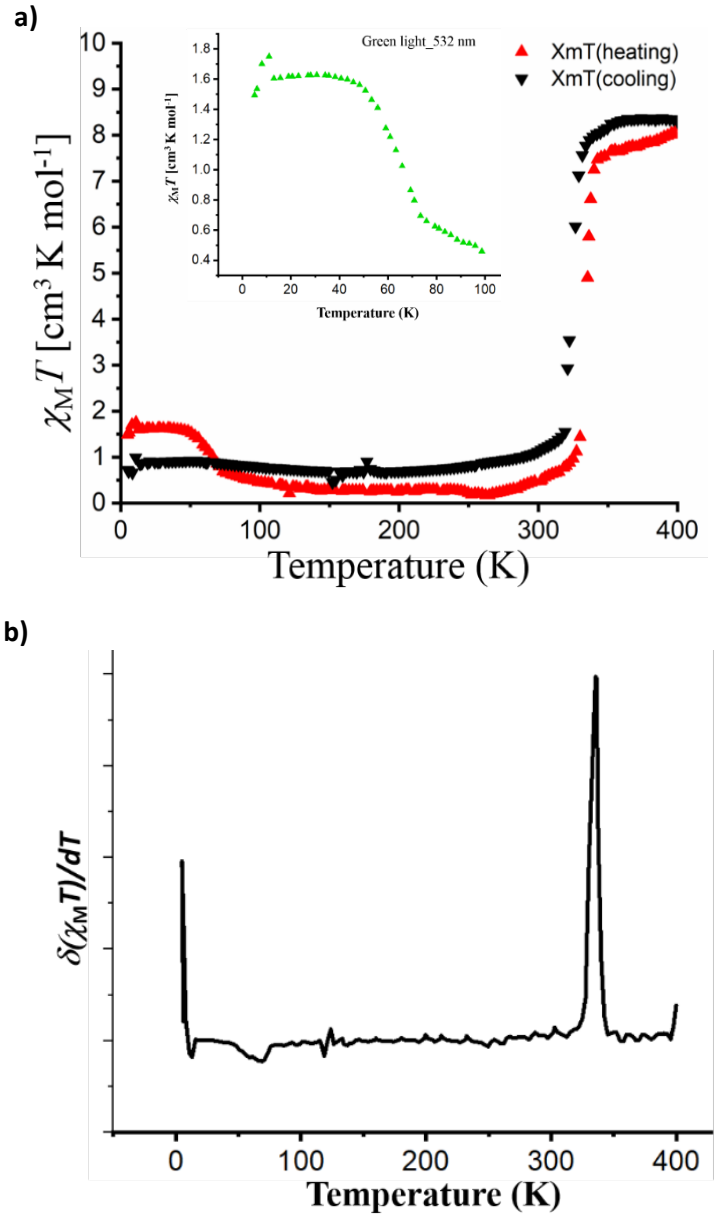

Figure S10. a) $\chi_M T$ *vs* T plot for 1 with light irradiation at 5 K with 532 nm wavelength followed by temperature sweep up to 400 K (Inset: Enlarged view at low temperature after light irradiation) b) Derivative plot of $\chi_M T$ *vs* T plot.

7. **Thermogravimetric Analysis Study:**

a)

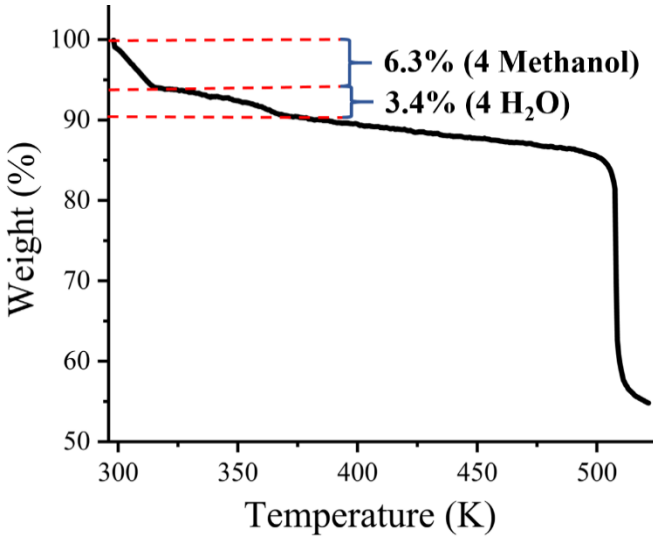

b)

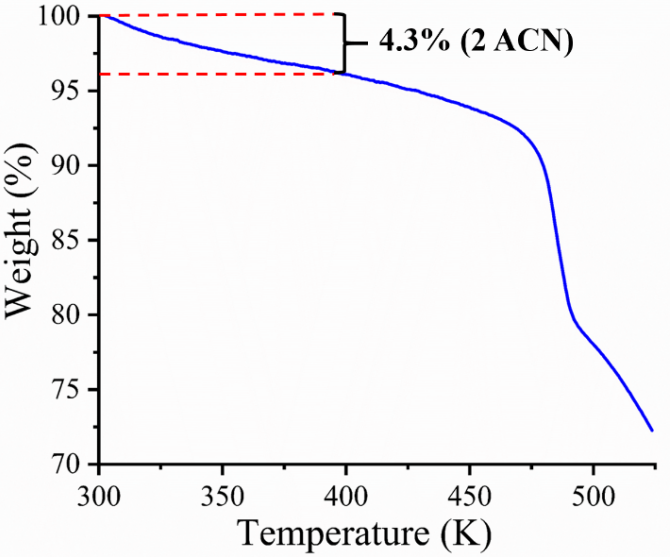

c)

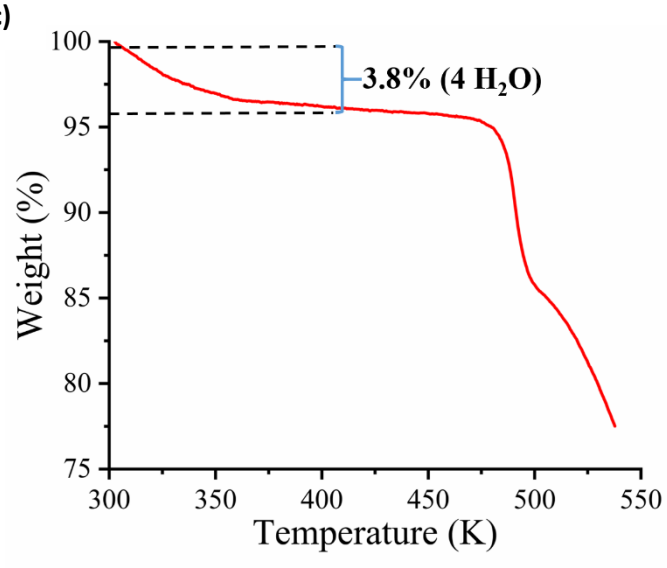
3.8% (4 H2O)
Weight (%)
Temperature (K)
100
95
90
85
80
75
300
350
400
450
500
550

d)

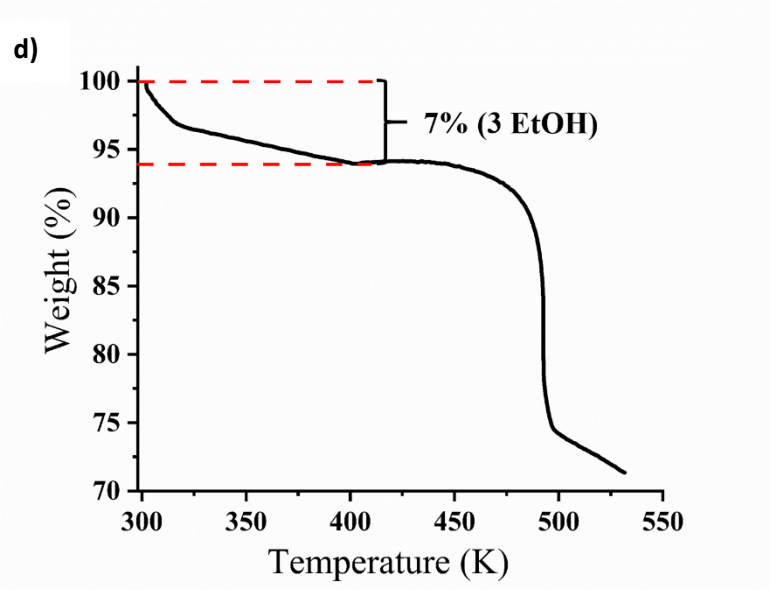
7% (3 EtOH)
Weight (%)
Temperature (K)
100
95
90
85
80
75
70
300
350
400
450
500
550

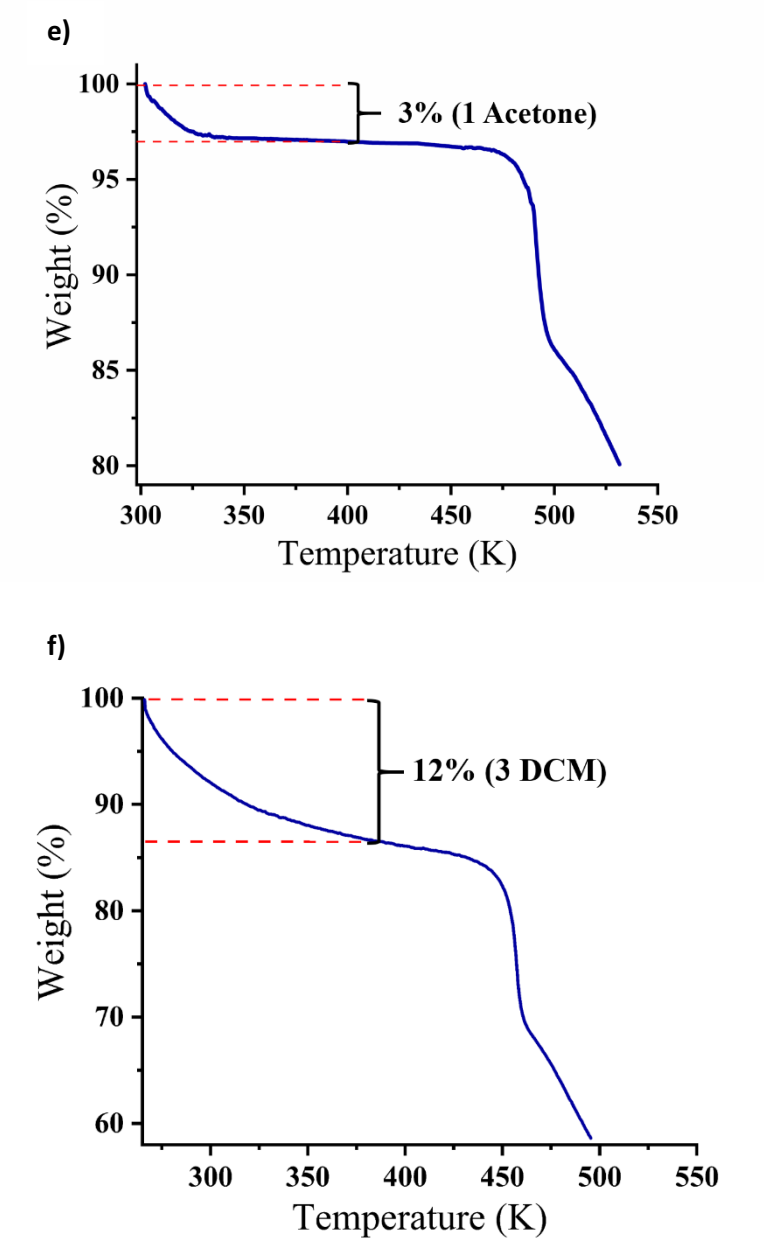

Figure S11. TGA data for the complexes a) **1**•4MeOH•4H_2O, b) **1**•2MeCN, c) **1**•4H_2O, d) **1**•3EtOH, e) **1**•Acetone and f) **1**•3DCM.

8. **FT-Infrared Spectroscopy study:**

a)

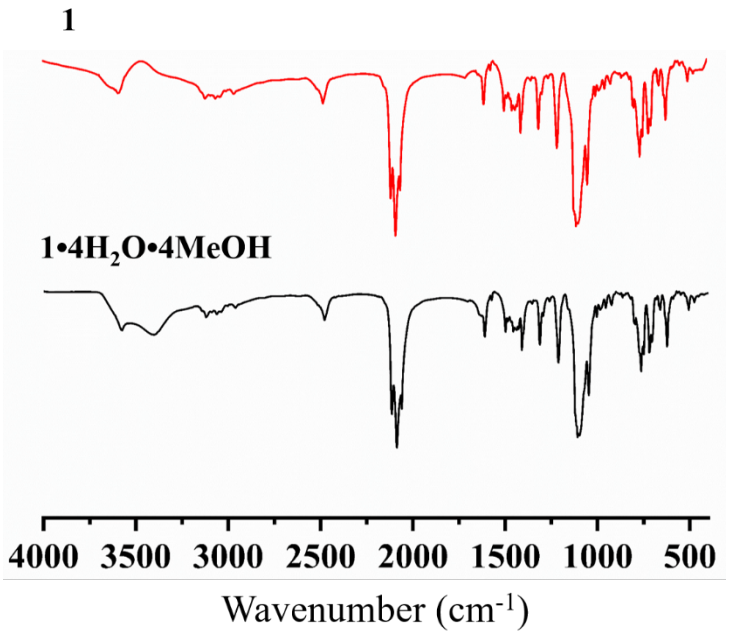

b)

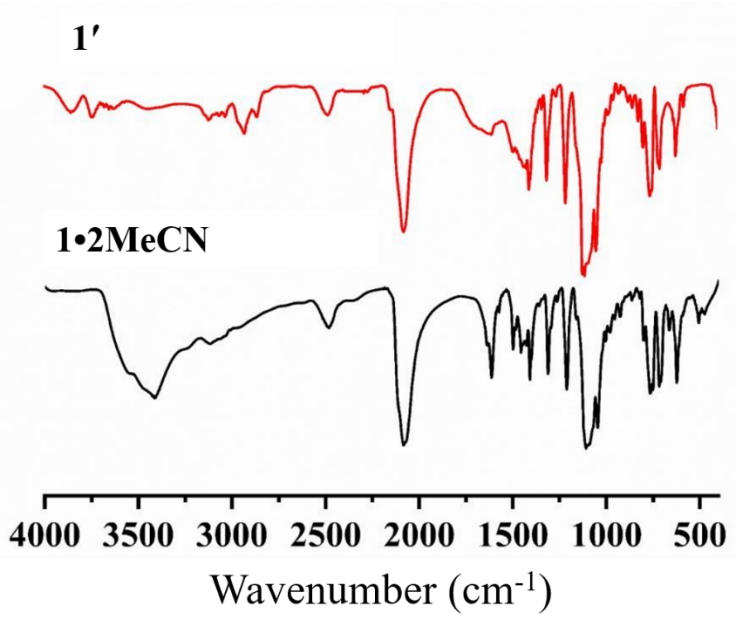

c)

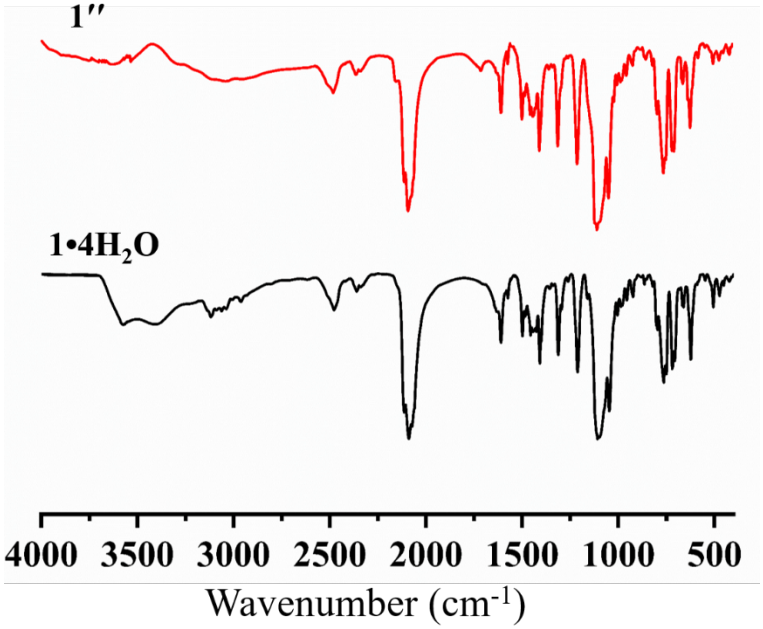
1''
1•4H2O
4000 3500 3000 2500 2000 1500 1000 500
Wavenumber (cm-1)

d)

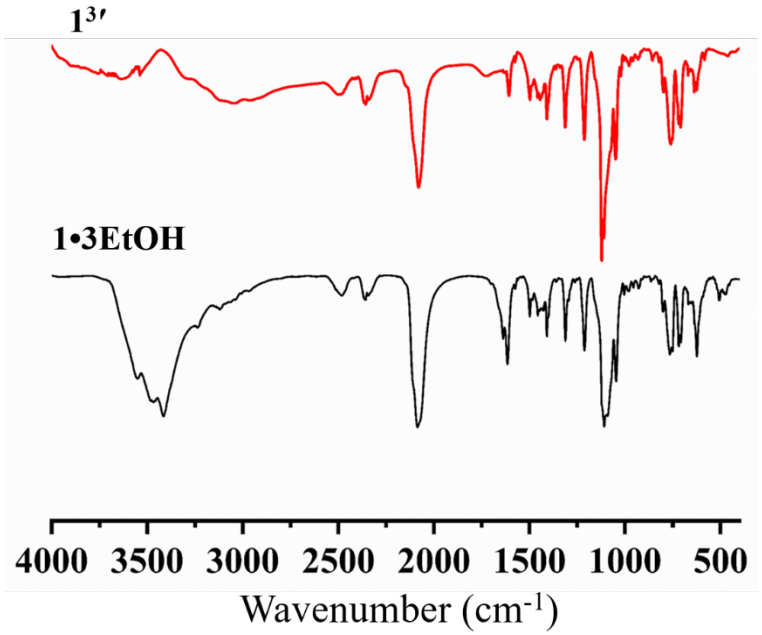
1³'
1•3EtOH
4000 3500 3000 2500 2000 1500 1000 500
Wavenumber (cm-1)

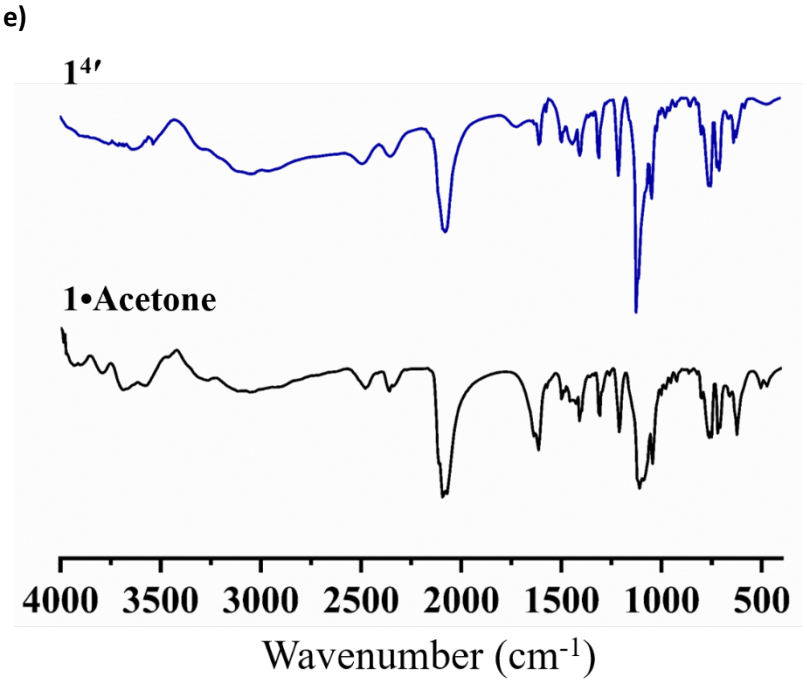

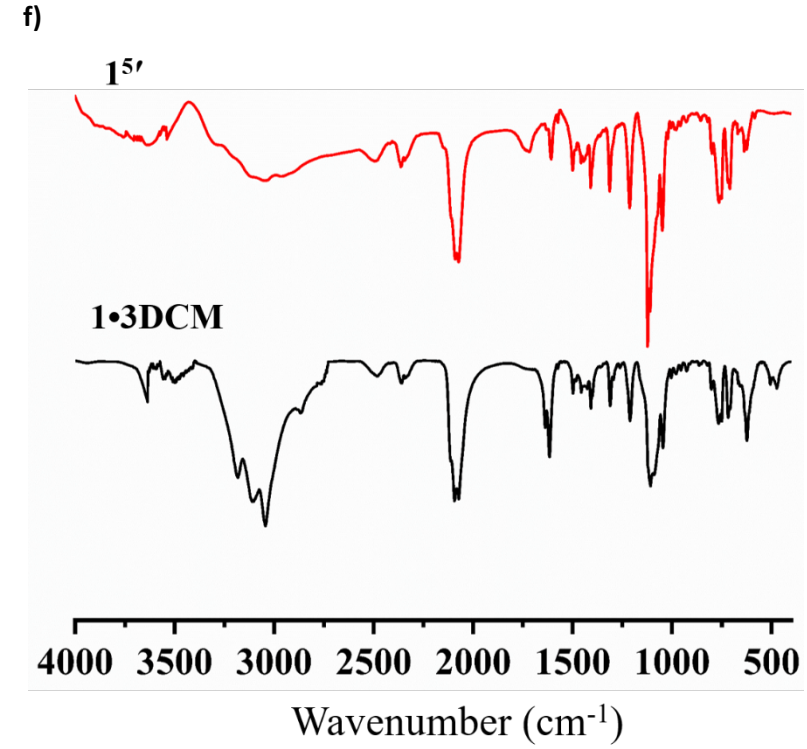

Figure S12. FT-IR data for the complexes a) **1**•4H_2O•4MeOH & **1**, b) **1**•2MeCN & **1'**, c) **1**•4H_2O & **1"**, d) **1**•3EtOH & **1³′**, e) **1**•Acetone & **1⁴′** and f) **1**•3DCM & **1⁵′**.

9. Variable Temperature Infrared Spectroscopy:

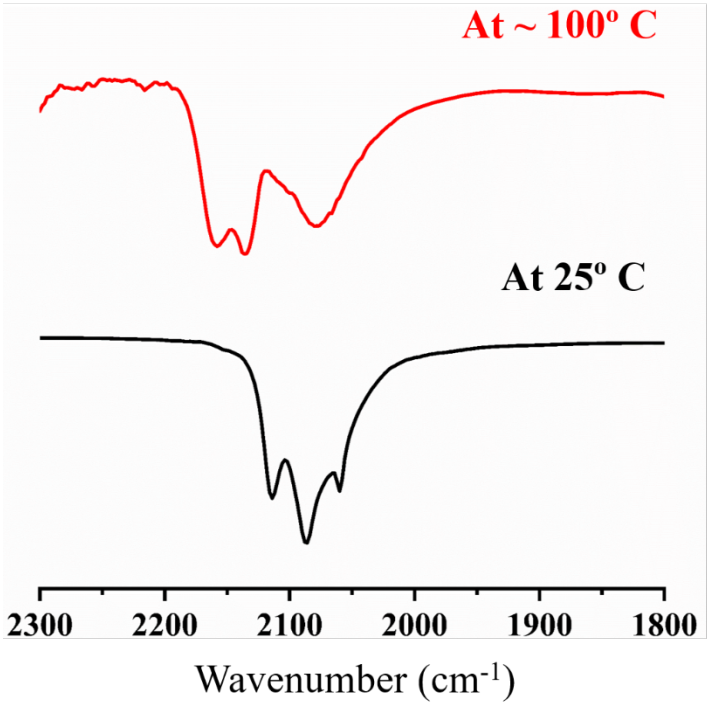

Figure S13. Infrared spectroscopy of **1**•4MeOH•4H_2O at Room temperature (25°C) and at ~100°C.

At 25°C, the IR spectrum shows peaks at 2116, 2087 and 2059 cm^{-1} corresponding to Fe^{II}-CN-Co^{III}, Fe^{II}-CN asymmetric and symmetric stretching frequency respectively. Upon heating the sample at about 100°C, the IR data shows appearance of two new bands at 2158 and 2134 cm^{-1} representing Fe^{III}-CN-Co^{II} and Fe^{III}-CN respectively.[4] While the peaks present at room temperature, although unresolved were also present in almost 50% ratio. This may be due to non-availability of the space for free expansion of complex compressed in KBr pellet.

10. Cyclic Voltammetry Study:

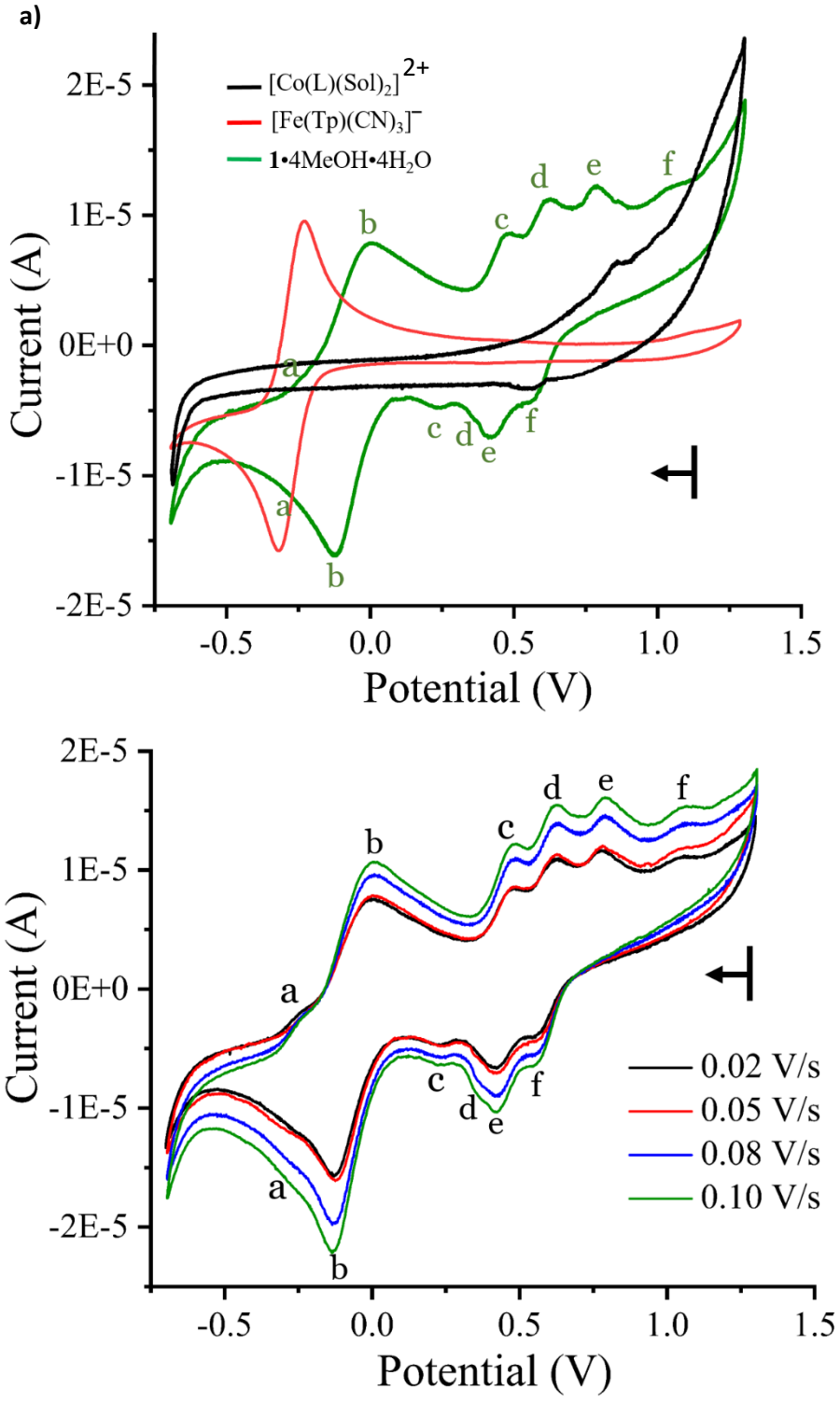

Figure S14. Cyclic Voltammetry of a) **1**•4MeOH•4H_2O and its component metal complexes and b) **1**•4MeOH•4H_2O at different scan rates.[5,6] The arrow represents the direction of sweeping of potential.

The cyclic voltammogram of $Na[Fe(Tp)(CN)_3]$ displays a reversible redox peak at -0.30 V and -0.21 V *vs* Fc/Fc^+ corresponding to reduction and oxidation around Fe(III) center ($Fe^{III/II}$ and $Fe^{II/III}$), respectively. Complex $[Co(L)(sol)_2]^{2+}$ gives a quasi-reversible peak at 0.65 V and 0.82 V *vs* Fc/Fc^+ showing reduction and oxidation at Co^{II} center ($Co^{II/I}$ and $Co^{I/II}$) respectively. A multiple approach for obtaining a good quality cyclic voltammetry for the Co-complex was unsuccessful. These may be because of instability of the complex in the solvent medium. For **1**•4MeOH•$4H_2O$, since it is present in $[Fe^{II}_{LS2}Co^{III}_{LS2}]$ state in solution phase at 298 K, the two merged peaks ranging between 0 V and below (negative potential) are ascribed as the two step oxidation of Fe^{II} center represented as $[Fe^{II}_2Co^{III}_2]/[Fe^{III}Fe^{II}Co^{III}_2]$ and $[Fe^{III}Fe^{II}Co^{III}_2]/[Fe^{III}_2Co^{III}_2]$. While the four merged quasi-reversible peaks ranging from 0.3 V to 1.05 V corresponds to partial stepwise reduction of Co^{III} center depicted as ($[Fe^{III}_2Co^{II}_2]/[Fe^{III}_2Co^{III}Co^{II}]$ and $[Fe^{III}_2Co^{III}Co^{II}]/[Fe^{III}_2Co^{III}_2]$.[5]

The peak differences between the Fe- and Co- precursor complexes and that of the complex **1**•4MeOH•$4H_2O$ in the control experiment (Figure S14a) shows that, the peaks present in the CV of **1**•4MeOH•$4H_2O$ is for the two sub-components bridged by the cyanide units forming the square complex. It is expected that the system is stable in the solvent medium.

11. UV-Visible Spectroscopy:

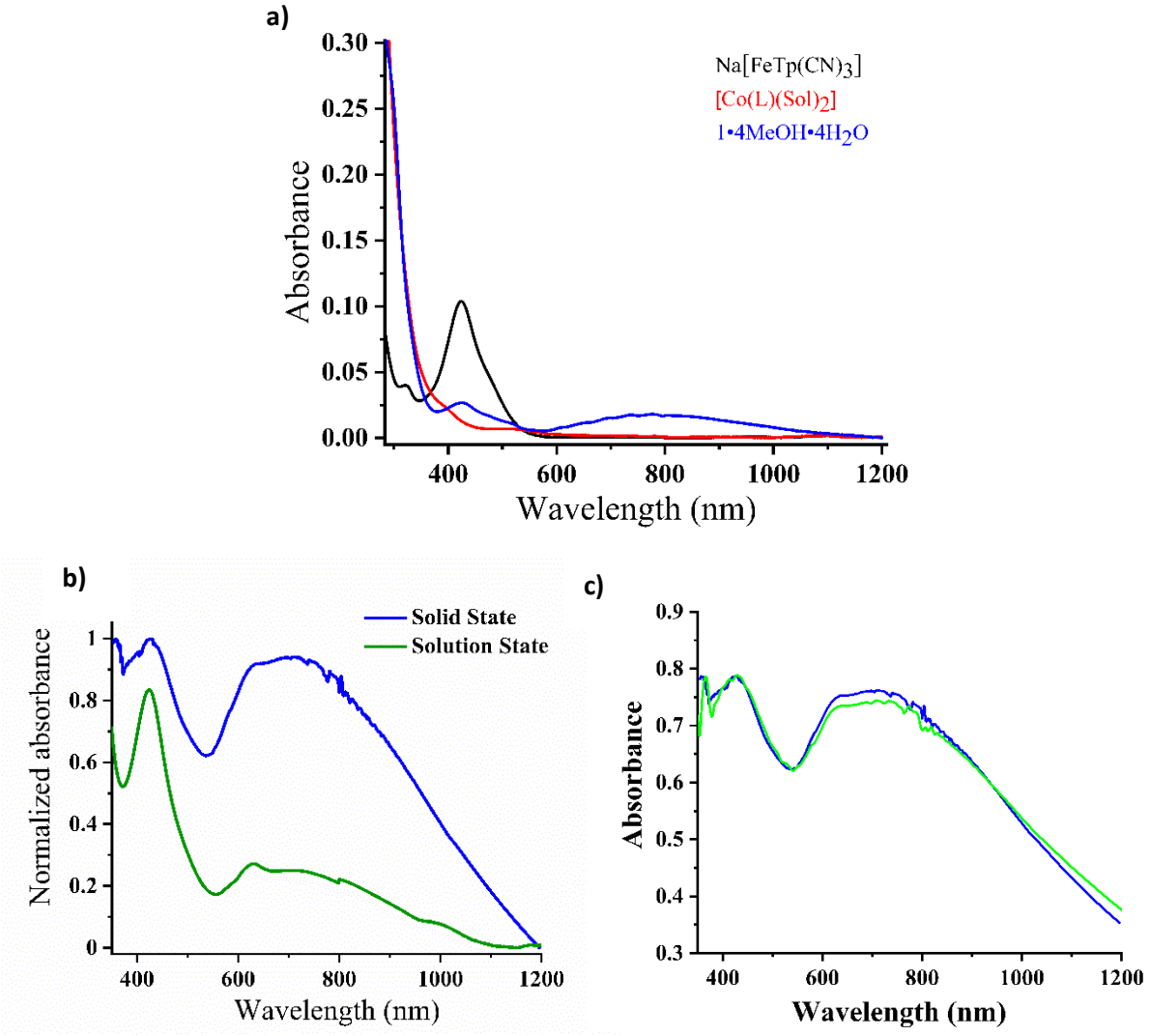

Figure S15. a) Solution state UV-Visible spectroscopy of **1**•4MeOH•4H_2O and its component metal complexes, b) Solution state (green) and solid state (blue) UV-visible spectroscopy for **1**•4MeOH•4H_2O and c) Solid state UV-visible spectroscopy for **1**•4MeOH•4H_2O (blue) and **1** (green).[5,7-8]

The stability of the complex in solution as well as solid phase is well supported by the similar solid and solution phase UV-Visible spectroscopic data. (Figure S15b)

References:

1 J. Kim, S. Han, I.-K. Cho, K. Y. Choi, M. Heu, S. Yoon and B. J. Suh, *Polyhedron* 2004, **23**, 1333-1339.

2 C. Ng, M. Sabat and C. L. Fraser, *Inorg. Chem.* 1999, **38**, 5545-5556.

3 (a) C. P. Slichter and H. G. Drickamer, *J. Chem. Phys.* 1972, **56**, 2142-2160; (b) W. Nicolazzi and A. Bousseksou, *C. R. Chimie* 2018, **21**, 1060-1074.

4 S. De, J.-R. Jiménez, Y. Li, L.-M. Chamoreau, A. Flambard, Y. Journaux, A. Bousseksou and R. Lescouëzec, *RSC Advances* 2016, **6**, 17456-17459.

5 M. Nihei, Y. Sekine, N. Suganami, K. Nakazawa, A. Nakao, H. Nakao, Y. Murakami and H. Oshio, *J. Am. Chem. Soc.* 2011, **133**, 3592-3600.

6 A. Kumar, S. S., P. Varshney, A. Paul and S. Jeyaraman, *Dalton Trans.* 2019, **48**, 11345-11351.

7 Y.-Z. Zhang, P. Ferko, D. Siretanu, R. Ababei, N. P. Rath, M. J. Shaw, R. Clérac, C. Mathonièr and S. M. Holmes, J. Am. Chem. Soc. 2014, 136, 16854-16864.

8 J. Mercurol, Y. Li, E. Pardo, O. Risset, M. Seuleiman, H. Rousselière, R. Lescouëzec and M. Julve, *Chem. Commun.* 2010, **46**, 8995-8997.